3.2.8 The phylogeny of *Anomalophylla*

Anomalophylla is known to occur only in the higher mountains of East Tibet and northern China. Most species occur in forest habitats, but also steppe habitats of the drier northern Tibetan highland, in a few cases also in meadows of the subalpine and alpine zone, occupying an overall altitudinal amplitude from 1000 to over 4600 meters. In higher latitudes the taxa occur at lower altitudes. Morphologically specialized high altitude specialists with reduced wings have not evolved. Specimens of *Anomalophylla* are active during daytime on plants, and similar to the species of *Omaloplia* or *Microserica*, with the same activity period, they show a notable colour polymorphism in dorsal surface.

Material and methods

Taxon sampling and characters

Thirty-four species belonging to six genera were included in the cladistic analysis, with *Comaserica bergrothi* chosen as the outgroup taxon due to their rather close relationship to the ingroup taxa, but with a high probability of not being part of the ingroup (chapter 3.1).

Character coding was based on 37 species belonging to seven genera (see appendix A 3.2.8). The choice of taxa to be included in the ingroup was mainly based on the most recent classification of the *Anomalophylla* species (Medvedev 1952b) and preliminarily hypothesized presumptive relatives, with numerous new species included additionally into *Anomalophylla* (Ahrens 2004b, this chapter). For *Anomalophylla tristicula tristicula*, two forms have been coded, the first being the typical one, and the second one (form B) has the basal lobe of right paramere possessing, additionally, a small convex secondary lobe medially. Sixty-eight adult characters were scored. The character states are illustrated in Figs 107-109.

Phylogenetic analysis

The 68 characters (47 binary and 21 multistate) were all unordered and equally weighted. Inapplicable characters were coded as „-", while unknown character states were coded as „?" (Strong and Lipscomb 1999). The parsimony analysis was performed in NONA 2.0 (Goloboff 1999) using the parsimony ratchet (Nixon 1999) implemented in NONA, run with WINCLADA vs. 1.00.08 (Nixon 2002) as a shell program. Two hundred iterations were performed (one tree hold per iteration) repeating the search ten times. The number of characters to be sampled for reweighting during the parsimony ratchet was determined to be six. All searches were done under the collapsing option "ambiguous" which collapses every node with a minimum length of 0. State transformations were considered to be apomorphies of a given node only if they were unambiguous (i.e., without arbitrary selection of accelerated or delayed optimization) and if they were shared by all dichotomised most parsimonious trees.

Bremer support (Bremer 1988, 1994) and bootstrap values (Felsenstein 1985) were evaluated using NONA. Bootstrap analyses of data were performed with 200 replicates using TBR branch swapping. The search was set to a Bremer support level of 12, with seven runs (each holding a number of trees from 100 to 500 times multiple of suboptimal tree length augmentation) and a total hold of 8000 trees. Character changes were mapped on the consensus tree using WINCLADA.

Successive weighting (Farris 1969) was used to further evaluate phylogenetic relationships. This method uses *post hoc* character weighting based on the fit of each character as applied to the trees currently in memory. Thus, the 'quality' of the character data is used rather than intuitive feeling regarding weighting of characters. Although this method

increases the assumptions in the analysis (Siebert 1992), it is useful for analysing phylogenetic pattern when characters exhibit a high level of homoplasy. Characters were reweighted based on the consistency index and retention index. The base weight was set at 100. Weights were inserted into NONA parsimony ratchet search via the WINCLADA surface manually. Tree searches continued until the character weights no longer changed (Farris 1988) or until identical trees were found in consecutive searches (indicating stability in the trees).

Characters and character states

In describing character states, I refrain from formulating any hypothesis about their transformation. In particular, coding does not implying whether a state is derived or ancestral. The data matrix is presented in the appendix B 3.2.8.

Head

1. *Labroclypeus widest*: (0) at base (Fig. 107L); (1) before base (Fig. 107M).
2. *Margins of labroclypeus*: (0) weakly reflexed (Fig. 107L); (1) strongly reflexed (Fig. 107M).
3. *Frons*: (0) glabrous or a few setae behind frontoclypeal suture only (Fig. 107L); (1) long and densely erectly setose behind frontoclypeal suture (Fig. 107S); (2) completely, long and densely erectly setose (Fig. 107T).
4. *Labroclypeus medially*: (0) flat; (1) moderately convex.
5. *Frontoclypeal suture*: (0) not elevated; (1) elevated (in proportion to frons and clypeus).
6. *Mentum anteriorly:* (0) convex; (1) weakly elevated and edged (Fig. 107N); (2) flat (Fig. 107O).
7. *Labial palpomeres*: (0) slender and long; (1) short and robust (Figs 107N,O).
8. *Number of antennomeres of club*: (0) six; (1) five; (2) four; (3) 1&2.
9. *Antennal club*: (0) shorter than labroclypeus maximal width or as long as labroclypeus maximal width (Figs 107A,B); (1) longer than labroclypeus maximal width (Figs 107C-G).

Thorax

10. *Pronotum, coloration in male*: (0) without polymorphism; (1) with polymorphism.
11. *Pronotal disc*: (0) glabrous (Figs 107A,B); (1) setose on anterior angles; (2) completely setose (Figs 107S, T).
12. *Pronotum, anterior angles*: (0) sharp, produced anteriorly (Fig. 107P, arrow); (1) rounded, produced anteriorly (Fig. 107Q, arrow); (2) rounded, not produced (Fig. 107R, arrow).
13. *Pronotum, basal marginal line*: (0) absent; (1) present, but fine.
14. *Pronotum, punctation*: (0) simple; (1) double.
15. *Pronotum, basal marginal line medially*: (0) present; (1) absent.
16. *Pronotum, coloration in female*: (0) black, without polymorphism; (1) reddish brown or black, with polymorphism (Figs 107H,J); (2) reddish brown without polymorphism.
17. *Prothorax, hypomeron ventrally*: (0) not produced; (1) produced.
18. *Metasternum, pilosity*: (0) short and sparse (Fig. 107U); (1) long and dense (Fig. 107V).
19. *Elytra, pilosity*: (0) absent (Figs 107A,B); (1) present on odd intervals only (Figs 107D-J); (2) present on all intervals (Fig. 107C).
20. *Elytra*: (0) without dark spots (Figs 107C-J); (1) with a single large spot behind middle (Fig. 107B, arrow); (2) with an anterior mesal and an posterior lateral spot (Fig. 107A, arrows).

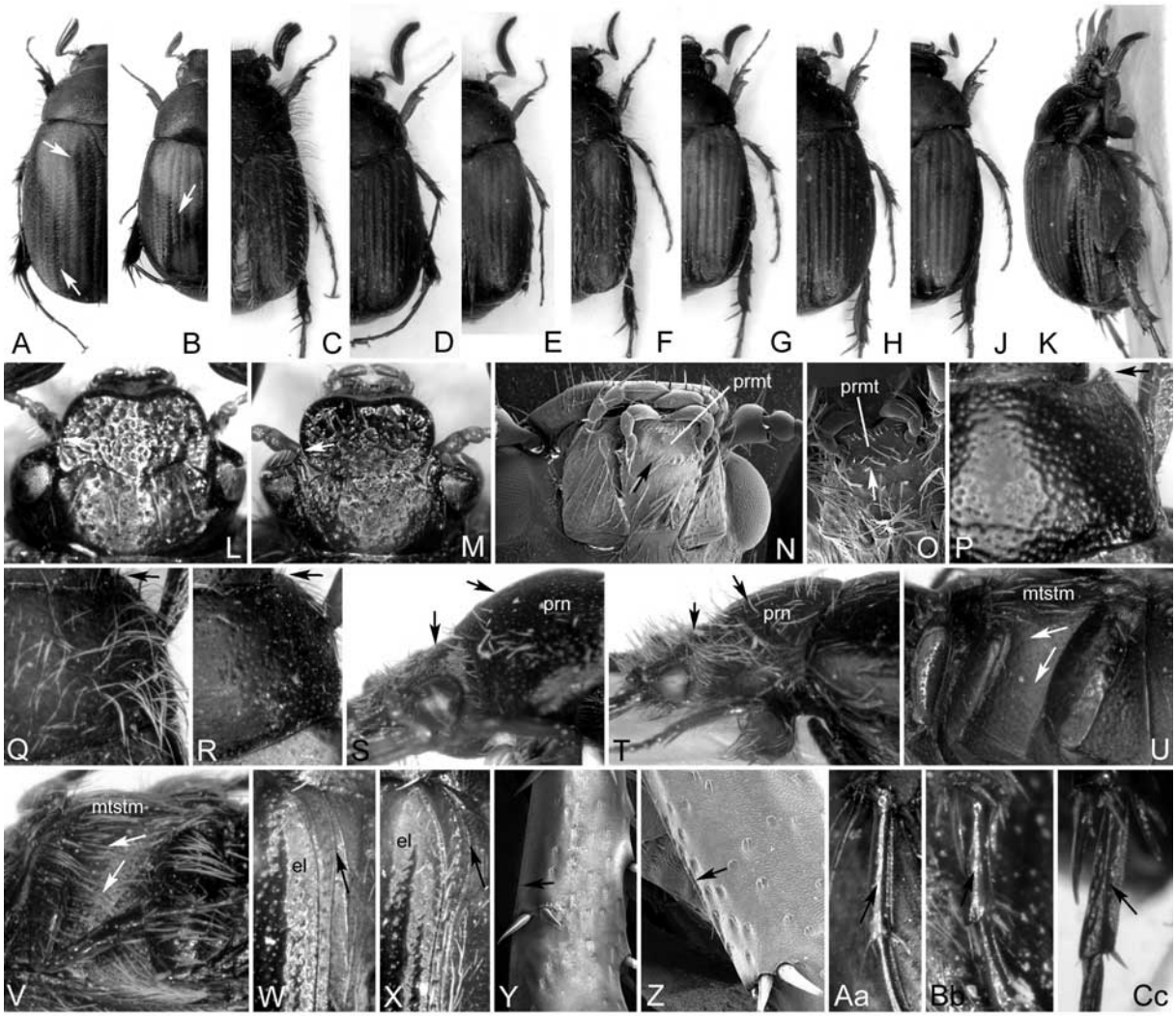

Fig. 107. A: *Microserica bhutanensis*; **B:** *Oxyserica brancuccii*; **C:** *Anomalophylla tristicula tristicula*; **D, E:** *A. dongchuanensis*; **F:** *A. liciata*; **G-K, M, N, R, S, X, Y, Cc:** *A. moxiensis*; **L, W:** *O. pygidialis pygidialis*; **O, Q, T, Z:** *A. moupinea*; **P:** *Sericania piattellai*; **U, Aa:** *M. interrogator*; **V, Bb:** *A. mandhatensis*. **A-J:** habitus, dorsal view (**A-G, K:** male; **H, J:** female); **K:** habitus, lateral view; **L, M:** head, dorsal view; **N, O:** prementum, ventral view; **P-R:** pronotum, right half, dorsal view; **S, T:** pronotum, lateral view; **U, V:** metasternum, ventrolateral view; **W, X:** basal half of elytra, lateral view; **Y:** metatibia, lateral view; **Z:** metatibia, lateral view (detail); **Aa-Cc:** basal metatarsomeres, lateral view (not to scale).

21. *Elytra, coloration*: (0) not polymorph (Fig. 107B); (1) polymorph (Figs 107A,D,E,H, J).
22. *Pilosity of even intervals*: (0) basally only; (1) on entire elytra.
23. *Setae on sutural interval*: (0) fine and short; (1) robust and long (Fig. 107F); (2) absent.
24. *Elytra, apical margin*: (0) with microtrichomes; (1) without microtrichomes.
25. *Elytra, punctation of intervals*: (0) almost evenly distributed (although concentrated along striae); (1) beside striae only.
26. *Elytra, ventral margin of epipleuron basally*: (0) weakly convex (Fig. 107W, arrow); (1) strongly convex (Fig. 107X, arrow).
27. *Elytra, pilosity*: (0) short (Figs 107G-K); (1) long (Figs 107C-F); (2) 0&1.
28. *Elytra, pilosity*: (0) sparse (Figs 107D,E,G-K); (1) dense (Figs 107C,F).

Legs

29. *Metacoxa*: (0) not enlarged (ratio metepisternum/ length of metacoxa: 1/ 1.23 – 1.6); (1) enlarged (ratio metepisternum/ length of metacoxa: > 1.7).
30. *Metatibia, medial face*: (0) smooth; (1) punctate.
31. *Metatibia, apical face*: (0) without interior spines; (1) with interior spines.

32. *Metatibia, apex interiorly close to tarsal articulation*: (0) bluntly angled, not truncate; (1) bluntly angled, weakly concavely sinuate; (2) moderately truncate; (3) sharply incised and strongly truncate.
33. *Metatibia, dorsal edge*: (0) not serrate (Fig. 107Z, arrow); (1) finely serrate (Fig. 107Y, arrow).
34. *Tarsi dorsally*: (0) smooth (Fig. 107Aa); (1) punctate (Fig. 107Cc).
35. *Basal tooth of interior protarsal claw*: (0) not widened in comparison to that of external claw; (1) widened in comparison to that of external claw.
36. *Metatarsomeres laterally*: (0) without carina (Figs 107Aa,Bb, arrow); (1) with a distinct carina (Fig. 107Cc, arrow).

Abdomen

37. *Pygidium*: (0) in both sexes dull; (1) in female at least apical half shiny.
38. *Pygidium, punctation*: (0) simple and moderately dense; (1) very large and dense.
39. *Pygidium, pilosity*: (0) apically present; (1) all over moderately dense; (2) all over dense.
40. *Pygidium in female*: (0) apically convex; (1) entirely flat; (2) flat, apically with a small convex elevation; (3) strongly convex medially.
41. *Tegument of abdominal sternites* (60x magnification): (0) without fine meshes (Fig. 108D); (1) with fine meshes (each mesh ten times smaller than a normal puncture) (Figs 108B,C).
42. *Median longitudinal impression on last and penultimate segment of abdominal sternites*: (0) absent; (1) present (Fig. 108A, arrows).

Male genitalia

43. *Phallobase*: (0) asymmetrical, at least apically (Figs 108E,H,K, 109M-V); (1) entirely symmetrical (Figs 108G, 109A).

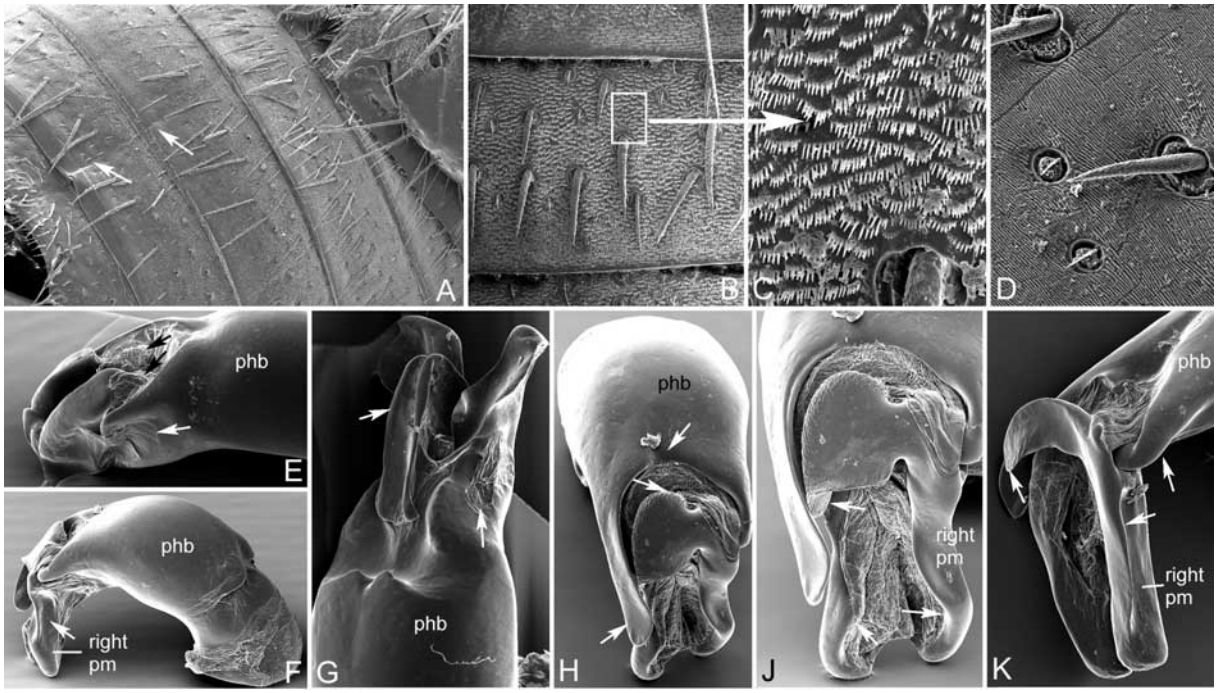

Fig. 108. A, K: *Anomalophylla tristicula tristicula*; **B, C, F, H, J:** *A. moxiensis*; **D, E:** *Microserica interrogator*; **G:** *Oxyserica bimaculata*. **A-D:** abdominal sternites, ventral view (**B-D:** detail); **E, G:** apical aedeagus, dorsolateral view; **F:** aedeagus, lateral view; **H:** apical aedeagus, dorsal view; **J:** parameres, dorsal view; **K:** parameres, lateral view (not to scale).

44. *Aedeagus, pair of dorsal sacks in membranous portion before distal ostium of phallobase*: (0) absent; (1) present (Figs 108E, black arrows, 108G, upper arrow, 109A, arrow).
45. *Sclerotized portion of ventral phallobase apically*: (0) deeply and narrowly sinuate; (1) weakly and widely sinuate; (2) convexly produced.
46. *Phallobase laterally between insertion of parameres and ventral sclerotization*: (0) not sinuate (Fig. 108K, upper right arrow); (1) sinuate (Figs 108E, white arrow, 108G, lower arrow).
47. *Phallobase laterally at left side*: (0) not produced (Fig. 108G); (1) weakly produced (process not longer than the maximal width of left paramere) (Figs 109D, arrow, M,N); (2) strongly produced (process longer than the maximal width of left paramere) (Figs 108H, lower arrow, J,K, 108E, arrow, F,O,Q,R,T-V).
48. *Insertion of left paramere*: (0) on the same level with the right paramere (Fig. 109A); (1) displaced distally compared to the right (Figs 108J,K, 109M-V); (2) displaced moderately basally compared to the right (Fig. 109L, upper arrow).
49. *Phallobase dorsomesally*: (0) without longitudinal impression (Fig. 108E); (1) with longitudinal impression (Figs 108H, upper arrow, 109O,T, both upper arrow).
50. *Parameres*: (0) asymmetrical (Figs 108E,H-K, 109B-V); (1) symmetrical (Figs 108G, 109A).
51. *Right paramere*: (0) without basal lobe (Figs 108E,G, 109A,L,M); (1) with basal lobe (Figs 108H,K, 109N-V); with basal lobe reduced in size (Fig. 109M, arrow).
52. *Right paramere medioapically*: (0) not sinuate (Figs 109M-S,U); (1) sinuate (Figs 108J, lower arrow, 109T,V).
53. *Right paramere at least in basal half*: (0) without sharp lateral carina (Figs 108F, arrow, 109K, arrow); (1) with sharp lateral carina (Figs 108K, lower arrow, 109G-J (arrow)).
54. *Passage from paramere to basal lobe*: (0) indistinct, lobe evenly narrowed from base to apex (Fig. 109N); (1) distinct, abruptly narrowed basally (Figs 108J,K, 109O,Q-V).
55. *Right paramere apically*: (0) not narrowed (Figs 108J,K, 109L,O, lower right arrow, R-V); (1) narrowed (Figs 109A,M,N,P,Q,S, lower right arrow).
56. *Basal lobe of right paramere medially*: (0) with a convex secondary lobe (Fig. 109R, right arrow); (1) without any secondary lobe (Figs 109N-Q).
57. *Basal lobe of right paramere*: (0) reaching the external margin of the left paramere (Figs 108J, left arrow, 109O,Q-U); (1) reaching at least the internal margin of the left paramere (Figs 109N,P,V).
58. *Apex of basal lobe of right paramere*: (0) directed medially (Fig. 109O); (1) directed distally (Figs 109Q,R,U,V); (2) directed basally (Figs 109M,N,P).
59. *Basal lobe of right paramere distally*: (0) not widened (Figs 108K, 109M-S); (1) widened (Figs 108J, 109H,T,V).
60. *Basal margin of basal lobe of right paramere*: (0) simple (Figs 108J,K, 109M-U); (1) reflexed and distally produced (Fig. 109V).
61. *Basal margin of basal lobe of right paramere*: (0) simple (Figs 108K, 109M-T); (1) convexly produced (Figs 108H, upper arrow, 109H,U).
62. *Margin of basal lobe of right paramere*: (0) smooth (Fig. 108K); (1) serrate (Fig. 108J).
63. *Right paramere at middle*: (0) straight (or not curved externally) (Figs 109N-S); (1) curved externally (Figs 108J, 109T).
64. *Parameres apically*: (0) evenly narrowed or rounded (Figs 108J, 109M,N,P-V); (1) obtusely widened (Figs 108K, 109O, arrows).
65. *Left paramere* (*dorsal view*): (0) apically narrowed (Fig. 109A); (1) with mostly subparallel sides (Figs 109M,Q,O,S); (2) abruptly widened medioapically from the middle (Figs 108J, 109T-V).

66. *Left paramere* (*dorsal view*): (0) straight (Figs 109S,T,N,P); (1) evenly curved (Figs 109O,M,U,V); (2) slightly angled at middle (Figs 109Q,R, arrow).
67. *Left paramere before distal medial extension*: (0) not sinuate (Fig. 109T, lower arrow); (1) deeply sinuate (Figs 109U, right lower arrow, 109V, upper arrow).
68. *Left paramere with distal extension*: (0) at base (Fig. 109F, arrow); (1) at middle (Fig. 109V, upper arrow); (2) before apical third (Figs 109T,U).

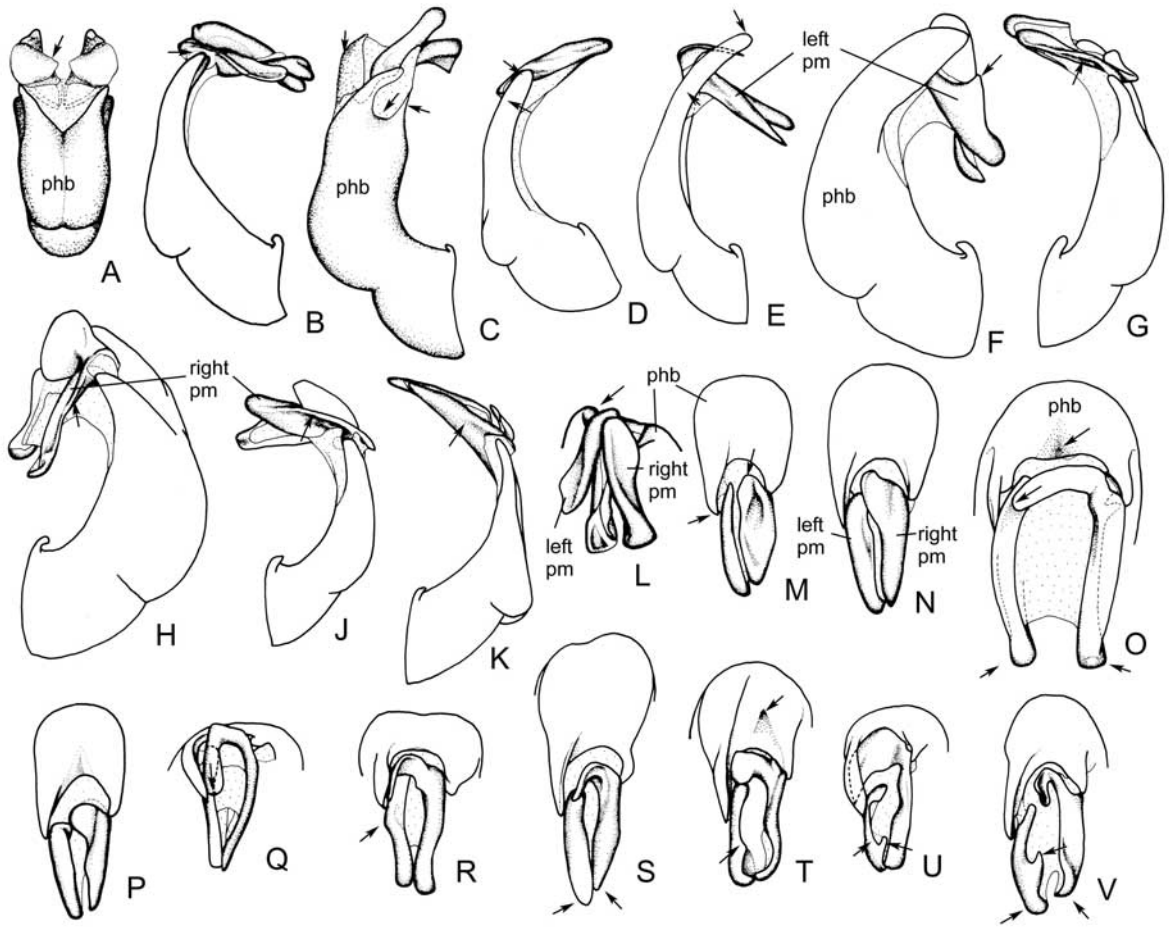

Fig. 109. A: *Oxyserica pygidialis pygidialis*; **B, L:** *Microserica steelei*; **C:** *M. arunensis*; **D, M:** *Anomalophylla morula*; **E, Q:** *A. stoetzneri*; **F, H:** *A. wulingshanica*; **G, V:** *A. ganhaiziensis*; **J, U:** *A. liciata*; **K, S:** *A. vidua*; **N:** *A. hispidulosa*; **O:** *A. tristicula tristicula*; **P:** *A. mandhatensis*; **R:** *A. moupinea*; **T:** *A. kozlovi*. **A:** aedeagus, dorsal view; **B-F:** aedeagus, left side lateral view; **G-K:** aedeagus, right side lateral view; **L-V:** parameres, dorsal view (not to scale).

Results

The analysis of 68 adult characters with the parsimony ratchet and the above mentioned settings repeating the search ten times yielded 127 equally parsimonious trees of 218 steps (ensemble consistency index (CI): 0.42, ensemble retention index (RI): 0.71). Characters 20 and 24 proved uninformative in the present data set. The strict consensus of these trees is presented in Fig. 110 with areas of conflict in topology shown as polytomies. The strict consensus tree (Fig. 110) of equally weighted characters exhibits a high level of polytomy, in basal as well as in apical nodes (*Anomalophylla*). This is attributed to the limited number of characters available for the comparative morphological analysis, but it is also obvious that suitable characters to resolve tree topology at all nodes are not present among the morphological character set.

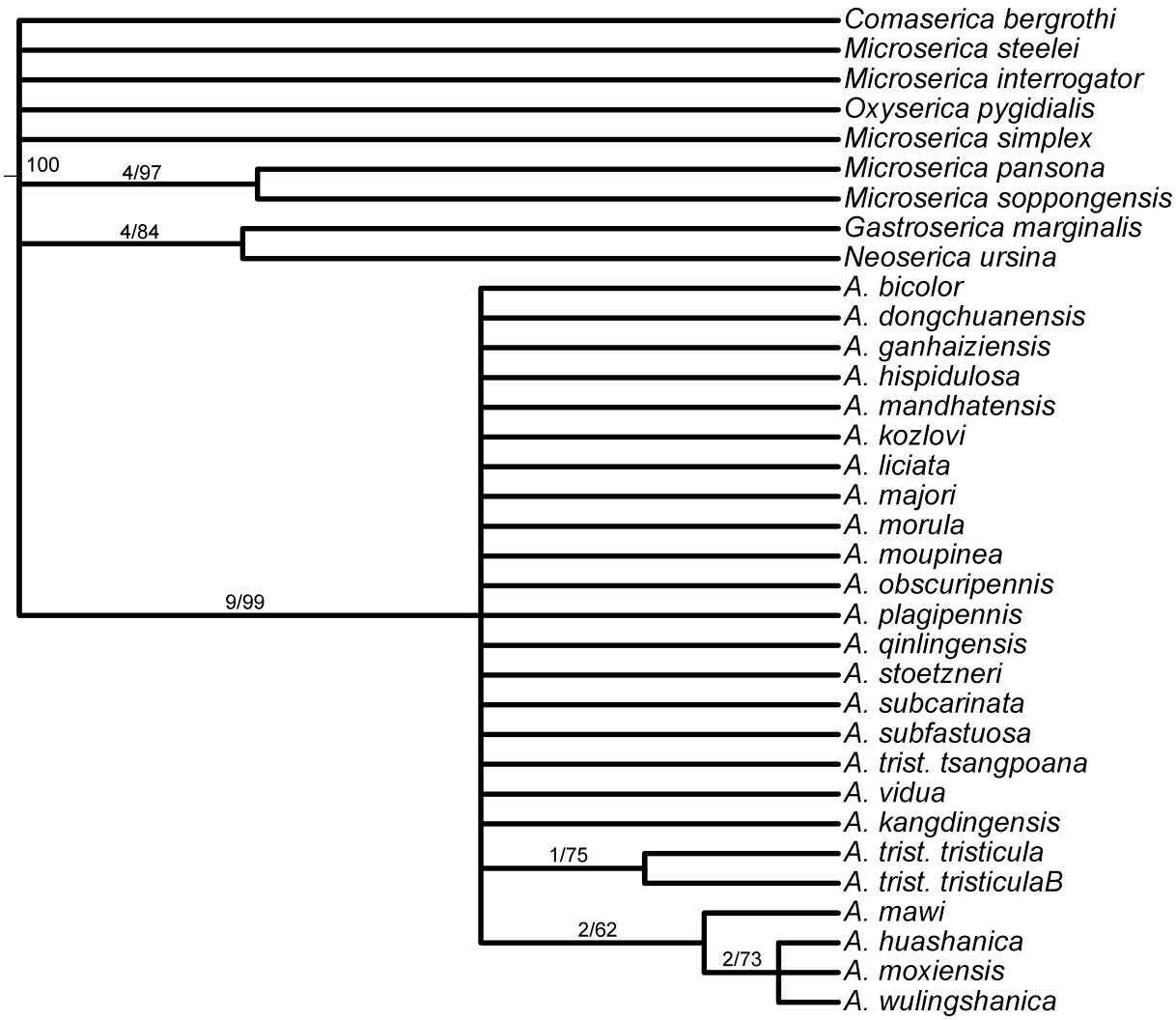

Fig. 110. Strict consensus (338 steps) of the 127 most parsimonious trees with a length of 218 steps (CI: 0.42, RI: 0.71); above each branch support indices (Bremer support/ bootstrap values).

Three monophyletic lineages may be recognized from the strict consensus tree (Fig. 110) within the ingroup: (1) *Anomalophylla*; (2) *Gastroserica* + *Neoserica*; (3) *Microserica soppongensis* + *M. pansona*. Monophyly of *Microserica* species included in this analysis was not apparent according to the tree topology. To assume in some manner information of the high number of equally parsimonious trees resulted from the parsimony ratchet with equally weighted characters, a majority rule consensus tree was generated (Fig. 111).

The use of successive approximations character weighting (SACW, Farris 1969) based on consistency index greatly reduced the number of most parsimonious trees (MPTs), producing a significantly more resolved strict consensus tree, especially among the representatives of *Anomalophylla*. The shortest trees were found with SACW based on the retention index (ri). In this approach weights no longer changed after three iterations (appendix C 3.2.8). From the SACW analysis result nine MPTs of 222 steps (CI: 0.44, RI: 0.78), whose strict consensus tree had the same length (Fig. 112). Although numerous distal nodes are well supported, the bootstrap values for the major nodes are generally low. This reflects the difficulty in finding apomorphies which are less subject to homoplasy to support these clades. Although achieved after two iteration, MPTs based on SACW with consistency index (ci) were distinctly longer (224 steps, CI: 0.54, RI: 0.8). They were, consequently, abandoned for further discussion.

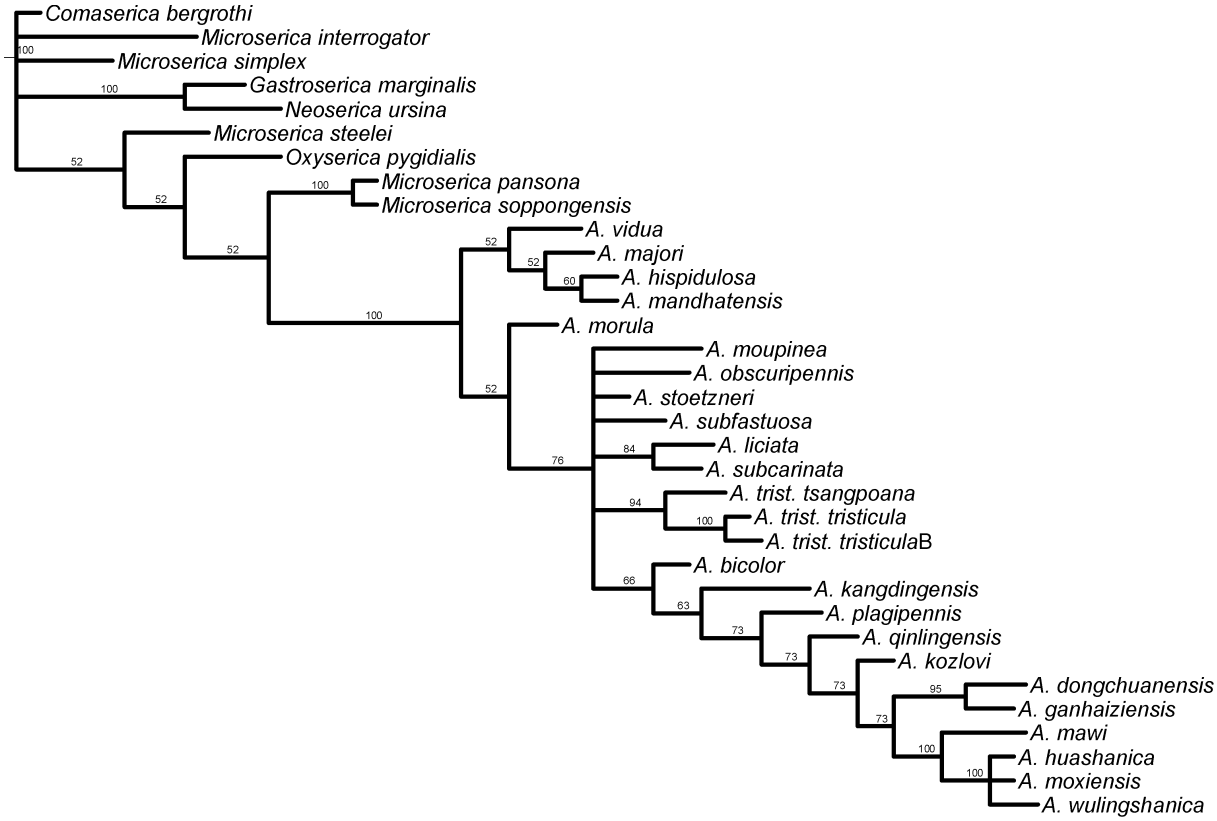

Fig. 111. Majority rule consensus (232 steps, CI: 0.39, RI: 0.68) of the 127 equally parsimonious trees (218 steps) resulted from parsimony ratchet based on equally weighted characters; above each branch percentage of a node among the number of the most parsimonious trees.

Discussion

Characters and computer analysis

The general structure of the equally weighted majority rule consensus tree (Fig. 111) shows some differences compared to the strict consensus tree of ri based SACW analysis (Fig. 112), which should be attributed to the fact that homoplasy plays a major role (CI: 0.42, RI: 0.71). While *Anomalophylla* is nested among the *Microserica* species (including *Oxyserica*) in the majority rule consensus tree (Fig. 111), from ri based SACW analysis the *Microserica* species (including *Oxyserica*) result monophyletic being the sister taxon to *Gastroserica* + *Neoserica*. The position of *Anomalophylla* in the strict consensus tree is basal, and consequently, this approach provides no evidence for the determination of the sister taxon of *Anomalophylla*. General topology among *Anomalophylla* varies only little between the analysis with unweighted characters and the analysis based on ri based SACW.

Characters of external morphology are in the same manner as male genital characters subject to homoplasy and consequently moderately consistent with the tree topology of the analyses, showing both similarly low means of consistency index (ci) and retention index (ri) (appendix C 3.2.8). Since there are no evident arguments available to choose a tree which offers a preferable hypothesis among the large number of MPTs from analysis with unweighted characters, the character evolution and the diversification of *Anomalophylla* are discussed, for the present, based on the ri based SACW strict consensus tree. Figure 113 illustrates the character evolution with the apomorphies given along each branch under WINCLADA optimization mode ‘unambiguous’ (showing unambiguous character changes only).

Monophyly of Anomalophylla

Although not exhaustive in terms of all principal sericine lineages included to examine the phylogenetic position, this study is the most comprehensive phylogenetic analysis of *Anomalophylla* ever conducted. The genus *Anomalophylla* once established by Reitter (1887) for a single species, *A. tristicula*, comprised so far only a few species from northern China and the eastern Tibetan Highland (Medvedev 1952b). These taxa have been even lumped to one species by Nikolaev (1982). In the meantime, the genus has been recorded for south-western Tibet (Ahrens 2004b) and many additional taxa have been discovered from eastern Tibet ranges.

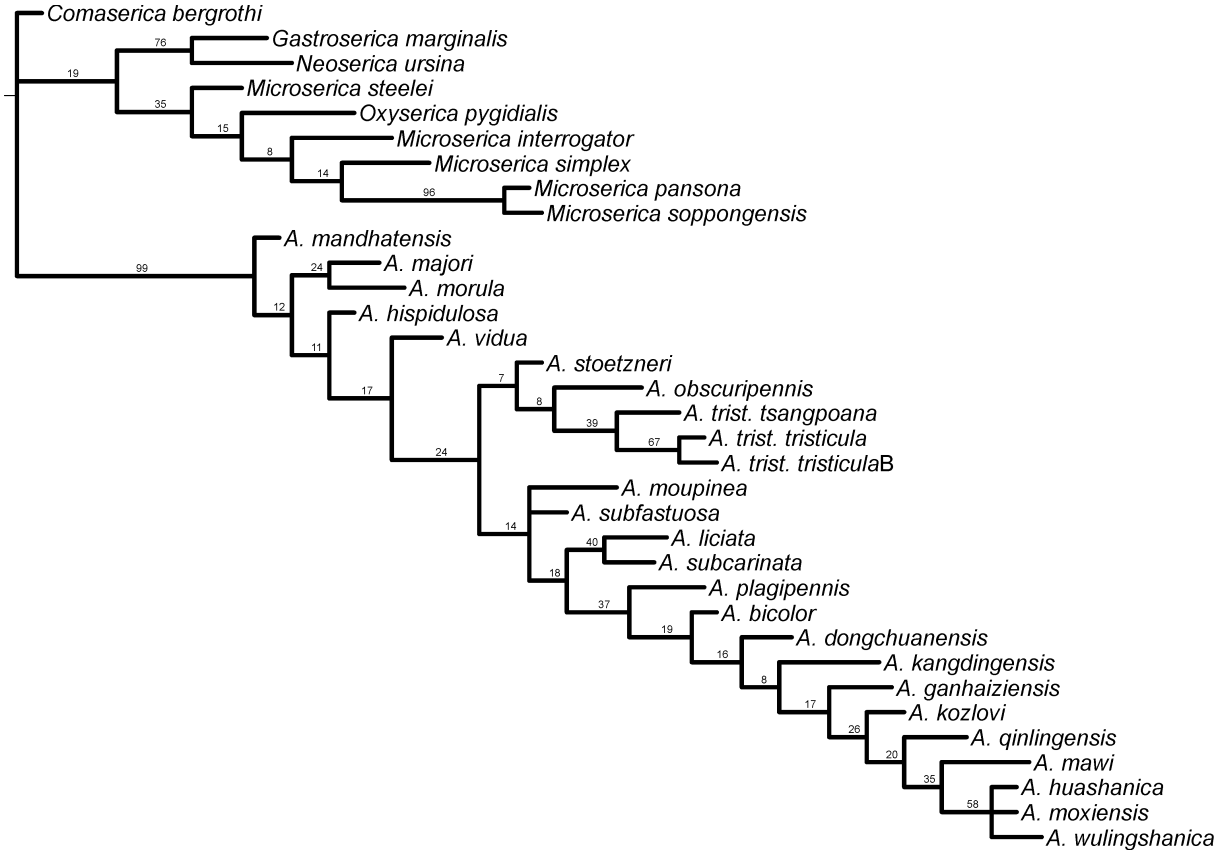

Fig. 112. Phylogeny of *Anomalophylla*. Strict consensus (222 steps, CI: 0.41, RI: 0.70) tree of nine equally parsimonious trees (222 steps, CI: 0.44, RI: 0.78) resulting from successive approximation based on retention index. Above each node branch support (bootstrap value) is indicated.

Monophyly of *Anomalophylla* was evident with highest branch supports in both analyses with unweighted (Fig. 110, Bremer support: 9, bootstrap value: 99 %) and weighted characters (Fig. 112, bootstrap value: 99 %). *Anomalophylla* is supported by a large number of unambiguous apomorphies. Among those not subject to homoplasy are (Fig. 113): (1) basal tooth of interior protarsal claw widened in comparison to that of external protarsal claw (35:1); (2) tegument of abdominal sternites (60x magnification) with fine meshes formed by microtrichomes (41:1); (3) median longitudinal impression on last and penultimate abdominal sternite present (42:1); and (4) phallobase laterally at left side (at least) weakly produced (47:1).

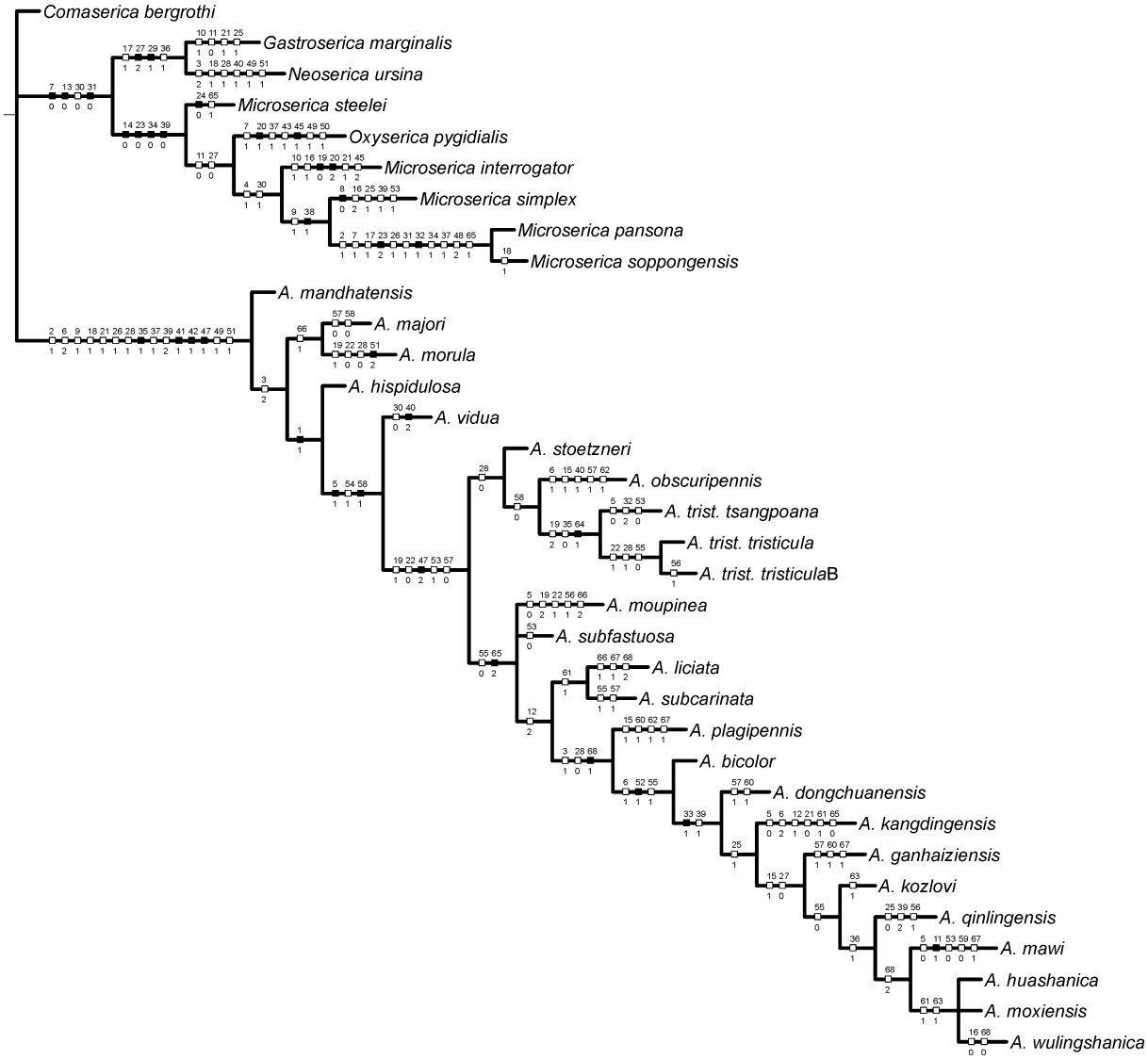

Fig. 113. Strict consensus (222 steps) tree of four MPTs (222 steps) resulting from successive approximation based on retention index which shows character changes and apomorphies mapped by state (discontinuous characters are mapped as homoplasy and only unambiguous changes are shown, unsupported nodes collapsed and using proportional branch lengths) (full squares: non-homoplasious character states; empty squares: homoplasious character states).

Evolution of Anomalophylla

The representatives of *Anomalophylla* exhibit among the fauna of the Himalaya and the Tibetan Plateau an interesting pattern of distribution. In connection with the phylogenetic hypothesis of the genus, this pattern may provide further information of the evolution of the highland fauna. All basal lineages (Fig. 114) occur in the south-eastern part of Tibetan highland, where the ranges of most species overlap or neighbour very closely. Interestingly, the most basal species, *A. mandhatensis*, extends its range furthest to the west, where (as far as known) it has an isolated occurrence close to the northern slope of the main Himalayan range at the north-western edge of Nepal. Due to the presumably harsh periglacial conditions during Pleistocene, and considering evidence of high age of the present elevation in southern Tibet (Spicer at al. 2003), I suppose that this occurrence is a result of a rather recent dispersal, perhaps during an interglacial stage or during later warm periods, such as in the middle Holocene (Gasse et al. 1991).

Although frequently recorded at the eastern slope of Tibet in humid habitats of the middle-montane belt, no *Anomalophylla* species occurs in very similar habitats at the southern slope of the Himalaya. A few taxa of more distal lineages, such as *A. kozlovi*, occur widely north-easterly, without, however, reaching the Japanese archipelago. Due to the presumably recent wide range expansion of *A. mandhatensis*, it should rather not be assumed that dispersal capacity of the species is limited. Consequently, a low age of *Anomalophylla* would be most consistent with the pattern of the phylogenetic hypothesis and the ranges of the species.

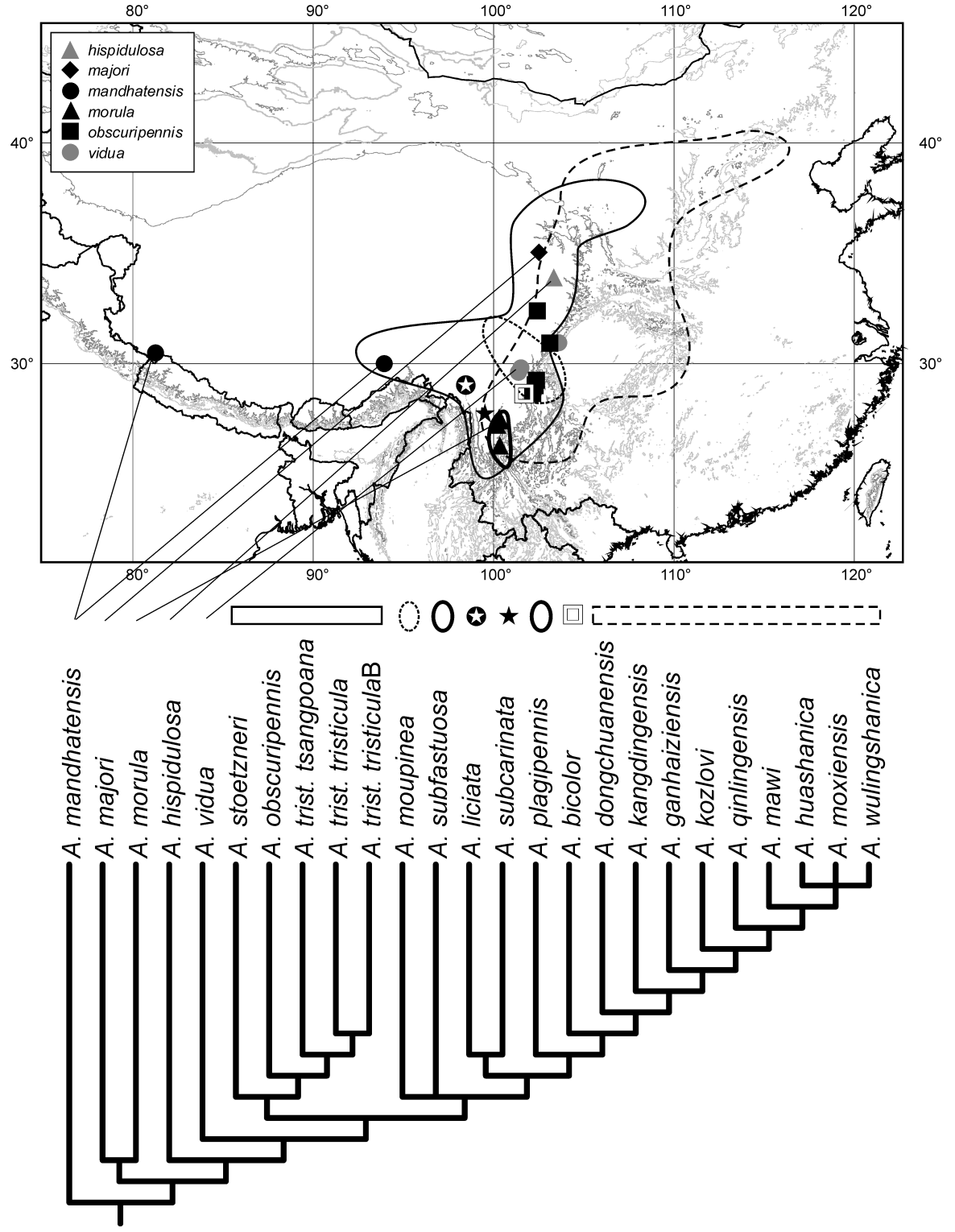

Fig. 114. Phylogeny of the *Anomalophylla* in its geographical framework, with indicated distribution of the species, and 1000 meter (light grey) and 2000 meter (dark grey) altitude line (*A.* = *Anomalophylla*).